A Novel Envelope Detector for High-Frame Rate, High-Frequency Ultrasound Imaging

Jin Ho Chang, *Student Member, IEEE*, Jesse T. Yen, *Member, IEEE*, and K. Kirk Shung, *Fellow, IEEE*

***Abstract*—This paper proposes a novel design of envelope detectors capable of supporting a small animal cardiac imaging system requiring a temporal resolution of more than 150 frames per second. The proposed envelope detector adopts the quadrature demodulation and the look-up table (LUT) method to compute the magnitude of the complex baseband components of received echo signals. Because the direct use of the LUT method for a square root function is not feasible due to a large memory size, this paper presents a new LUT strategy dramatically reducing its size by using binary logarithmic number system (BLNS). Due to the nature of BLNS, the proposed design does not require an individual LOG-compression functional block. In the implementation using a field programmable gate array (FPGA), a total of 166.56 Kbytes memories were used for computing the magnitude of 16-bit in-phase and quadrature components instead of 4 Gbytes in the case of the direct use of the LUT method. The experimental results show that the proposed envelope detector is capable of generating LOG-compressed envelope data at every clock cycle after 32 clock cycle latency, and its maximum error is less than 0.5 (i.e., within the rounding error), compared with the arithmetic results of square root function and LOG compression.**

I. Introduction

In conventional medical ultrasound imaging system, an envelope detector can be divided into two parts: extracting the magnitude of received echo signals and logarithmically compressing the magnitude information for efficient visualization. Although LOG-compression is usually implemented through a look-up table (LUT) method, the extraction of signal magnitude can be realized through various algorithms in hardware or software. A theoretical algorithm involves extracting an analytical signal from a received echo signal by Hilbert transform and computing its magnitude by square root of the sum of the squares of the real and the imaginary parts in the analytic signal. Although being capable of yielding the exact envelope and phase information from the analytic signal, this type of method is seldom used in commercial ultrasound imaging systems because of the involvement of a direct and an inverse Fourier transform requiring considerable overhead in processing time, which is both costly and more complex to implement. To realize the extraction of the analytic signal from the received echo data in real time, two different approximate Hilbert transform methods have been used: the finite impulse response (FIR) or infinite impulse response (IIR) Hilbert filter method [1], [2] and the time delay method [3], [4]. The algorithm most commonly used in commercial ultrasound imaging systems, however, is the quadrature demodulation technique generating the baseband in-phase and quadrature components of a received echo signal instead of the analytic signal [4]–[6].

The magnitude of either the analytic or the complex baseband signal is calculated through a square root function. The square root function can be realized by several algorithms [7]–[9]. In a small animal cardiac imaging system requiring very high frame rate, the square root function implemented by these algorithms must be capable of operation at very high speed. This is because the frame rate for the small animal cardiac imaging should be more than 150 frames per second [10], [11], thus the back-end processing, including a digital scan converter, should be performed in less than 6.7 ms for a frame. Because the envelope detection, including LOG-compression, usually is carried out in parallel with other back-end processing, the envelope detector can spend the entire time of 6.7 ms for its task. This means that the envelope detection for a scanline should be completed within 26.2 μs in the case of 256 scanlines. Hardware implementation of square root algorithms would support the requirement for small animal cardiac imaging at the expense of a high-cost, sophisticated design, especially for high-sampling frequency systems such as high-frequency ultrasound imaging systems [12]. However, software-based counterparts using a media processor [5] or a digital signal processor [6] demand very high-performance processors capable of high computational throughput, large internal memory, and high bandwidth of data transfer between internal and external memories. These requirements are predicated upon that accurate square root values can be obtained only by many iterative computations and data transfer operations that frequently occur to fetch LUT values and to store the results from/to external memories.

The LUT method is capable of providing the simplest implementation of the square root function and the fastest operation speed in both hardware and software if a fast and large-sized memory is available. Because the size of LUT exponentially increases with the number of input bits, the direct use of the LUT method to implement the square root function is hardly feasible even in a moderately accurate system. In the case of 16-bit representation each for real component and imaginary component and 8-bit representation for the output of the square root function, for

Manuscript received August 1, 2006; accepted April 10, 2007. This work was supported by NIH grant number R01-HL079976.

The authors are with the NIH Transducer Resource Center for Medical Ultrasonic Transducer Technology, Department of Biomedical Engineering, Los Angeles, CA (e-mail: jhchang@ieee.org).

Digital Object Identifier 10.1109/TUFFC.2007.463

example, LUT has 32-bit wide input and 8-bit wide output ports, so that it requires at least 4 Gbytes of memory ($2^{32} \times 8 \div 8$), which is currently impractical for a typical ultrasound imaging system.

This paper proposes a new design of the envelope detector including LOG-compression that adopts the quadrature demodulation and the square root function based on a new LUT strategy for high-frame rate, high-frequency ultrasound imaging systems. And the new LUT strategy used in the proposed design uses binary logarithmic number system (BLNS) [13]–[19] instead of the fixed-point number system. By using BLNS, the size of LUT can be dramatically reduced by the manipulation of square root equation, thus taking advantage of the attractive properties of the LUT method allowing fast operation speed and accuracy as well as simple implementation. Another merit of the new LUT strategy is that an individual LOG-compression functional block is not required. This is because the result from the square root function, represented by BLNS, is a LOG-compressed version of envelope information.

In this paper, the algorithms for the envelope detector and BLNS are described, and an example of the implementation of the proposed design in hardware is included, although the design also is suitable for software-based implementation. The operating time of the proposed design is estimated, and its accuracy is compared to that of an ideal envelope detector. The results show that the proposed design has a superior capability for high-frame rate, high-frequency ultrasound imaging system than the conventional envelope detectors.

II. Review of Algorithms for Envelope Detection

Envelope detection can be carried out by several algorithms classified into four types with different levels of accuracy and complexity. In this section, each type of algorithm is briefly described, and its accuracy is examined by computer simulation using MATLAB (MathWorks Inc., Natick, MA). In the simulation, 8-bit echo data from a 20-MHz, single-element transducer sampled at 500 MHz through the oscilloscope (Lecroy LC534, Chestnut Ridge, NY) were used. The −6 dB bandwidth of the transducer was 60%, and the echo data contained a second harmonic component of −40 dB level. The cutoff frequency of 33-tap low pass filters (LPF) used in the simulation was 12 MHz. The accuracy of each algorithm was quantified by using root mean square error (RMSE) between envelope data obtained by practical algorithms and the ideal Hilbert transformer. The RMSE values were normalized with respect to the root mean square (RMS) value of the ideal envelope data extracted by the ideal Hilbert transformer.

A. Ideal Hilbert Transformer

It is well-known that the received echo signal $r(n)$ sampled at an interval T_s can be expressed as:

$$r(n) = A(nT_s) \cdot \cos(n\omega_0 T_s + \phi_n), \tag{1}$$

where $A(nT_s)$ is the envelope information, ω_0 is the center frequency of the echo signal, and ϕ_n is phase angle varying with time. This received echo signal can be decomposed into its in-phase and quadrature components as:

$$\begin{aligned} r(n) &= A(nT_s) \cdot \cos(n\omega_0 T_s) \cdot \cos(\phi_n) \\ &\quad - A(nT_s) \cdot \sin(n\omega_0 T_s) \cdot \sin(\phi_n) \\ &= A_I(nT_s) \cdot \cos(n\omega_0 T_s) - A_Q(nT_s) \cdot \sin(n\omega_0 T_s), \end{aligned} \tag{2}$$

where $A_I(nT_s)$ and $A_Q(nT_s)$ represent the in-phase and the quadrature components of the received echo signal, respectively. By Hilbert transform, the analytic signal can be obtained:

$$r_a(n) = r(n) + j \cdot r_{\mathrm{HT}}(n), \tag{3}$$

where:

$$r_{\mathrm{HT}}(n) = A_Q(nT_s)\cos(n\omega_0 T_s) + A_I(nT_s)\sin(n\omega_0 T_s). \tag{4}$$

The envelope information can be obtained by computing the magnitude of (3) through the square root of the sum of the squares of $r(n)$ and $r_{\mathrm{HT}}(n)$. In this paper, the envelope data obtained from this ideal Hilbert transformer is used as a gold standard for the comparison of the accuracy of each algorithm.

B. Rectification of RF Signal Followed by Filter

Rectifying received echo signal is the simplest method for envelope detection. If phase angle ϕ_n is zero, (1) can be replaced by a Fourier series after taking absolute value [20]:

$$\begin{aligned} |r(n)| &= |A(nT_s)| \cdot |\cos(n\omega_0 T_s)| \\ &= A(nT_s) \cdot \left[\frac{2}{\pi} + \frac{r}{\pi} \sum_{k=1}^{\infty} \frac{(-1)^{k+1}}{4k^2 - 1} \cdot \cos(2kn\omega_0 T_s) \right], \end{aligned} \tag{5}$$

where it is assumed that the envelope information $A(nT_s)$ is a positive value. After low pass filtering with a cutoff frequency in a frequency interval determined by ω_0 and half bandwidth of the envelope signal, the envelope information is obtained as follows:

$$E(n) = [|r(n)|]_{\mathrm{LPF}} = \frac{2K}{\pi} \cdot A(nT_s), \tag{6}$$

where K is the gain of LPF. Although a median filter can be used in a software-based implementation instead of LPF [3], the accuracy of the LPF method is superior to that of the median filter method. This is clearly seen in Fig. 1 in which the envelope information of the received echo signal (gray dotted line) extracted by the rectifiers with a median filter (gray dashed-dot line), and LPF (dashed line) is presented. In order to quantify their accuracy, RMSE between the obtained envelope information and the ideal

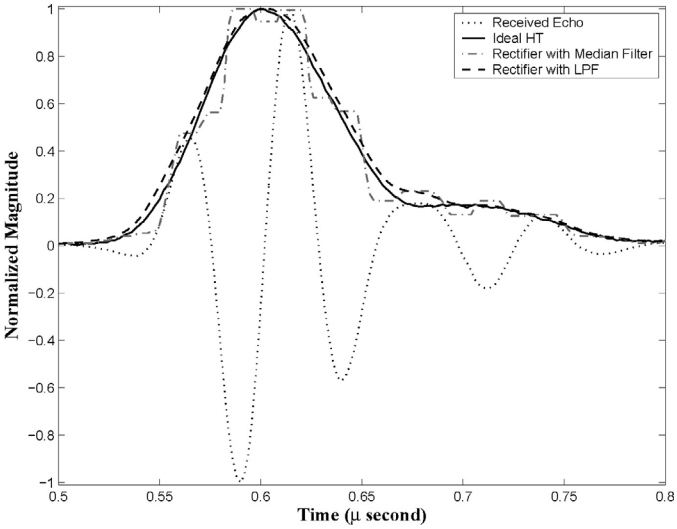

Fig. 1. Resultant the envelope information extracted from the rectifier with a median filter (gray dashed-dot line) and the rectifier with LPF (dashed line). As a gold standard for the comparison of the accuracy of each algorithm, the envelope information obtained from the ideal Hilbert transformer (solid line) is presented.

envelope information extracted by the ideal Hilbert transformer (solid line in Fig. 1) was calculated. The normalized RMSE values of the rectifier with a median filter and LPF were 13.35% and 7%, respectively.

In spite of its simplicity, this algorithm cannot be used for high-frequency ultrasound systems that uses the quadrature sampling technology to reduce sampling speed [4], [21]. Another drawback of this algorithm is that the second harmonic component of $A(nT_s)$ distorts the baseband signal obtained by taking the absolute value of the original echo signal. Furthermore, this algorithm always introduces aliasing caused by sampling because (5) is not a band-limited signal, although the magnitude of harmonic components generated by $\cos(2kn\omega_0 T_s)$ is drastically decreased with its order. In addition, this algorithm is hardly used in a commercial ultrasound system because it cannot provide phase information needed for Doppler and color flow imaging.

C. Approximate Hilbert Transformer

Because the transfer function of the Hilbert transformer has discontinuities at zero frequency and at half the sampling frequency, the direct utilization of the transfer function is impossible in time domain. As an approximate version, therefore, a well designed FIR or IIR Hilbert filter can be used to generate the Hilbert transformed data of the received echo signal [1], [2]. The block diagram of the envelope detector using the Hilbert filter is shown in Fig. 2(a). And the frequency response of a 33-tap FIR Hilbert filter used in the simulation is presented in Fig. 3. From the simulation results shown in Fig. 4, it is seen that the envelope information from this method (dashed line) comes close to the ideal envelope (solid line). The normalized RMSE value of this method was 6.21%, although it can be de-

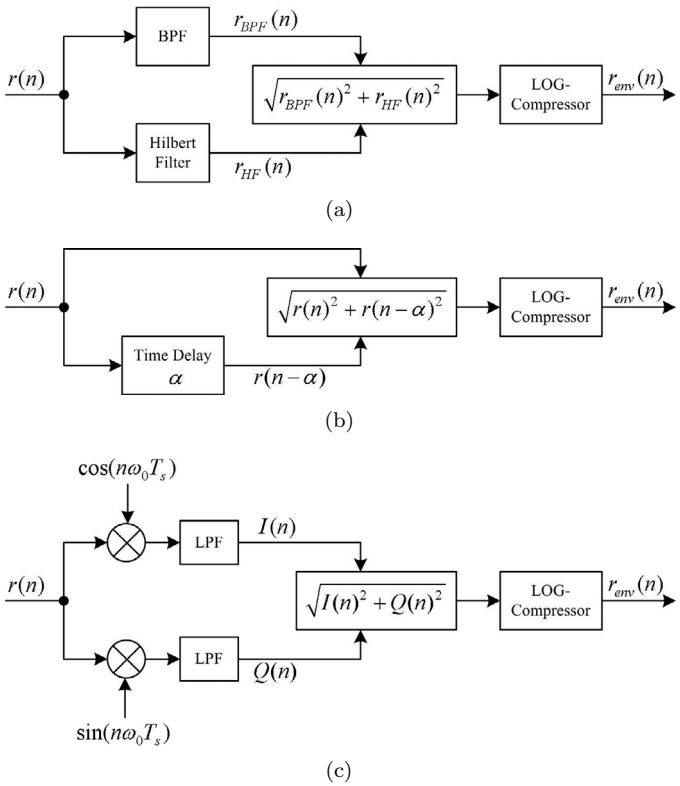

Fig. 2. Block diagram of the envelope detectors, including LOG-compression function by using the Hilbert filter method (a), the time delay method (b), and the quadrature demodulation method (c). $r(n)$ is a digitized echo signal, $r_{\mathrm{env}}(n)$ is LOG-compressed envelope information, α represents the number of delay samples corresponding to shifting a 90 degree phase from the center frequency ω_0 of the received echo data, and T_s is a sampling period.

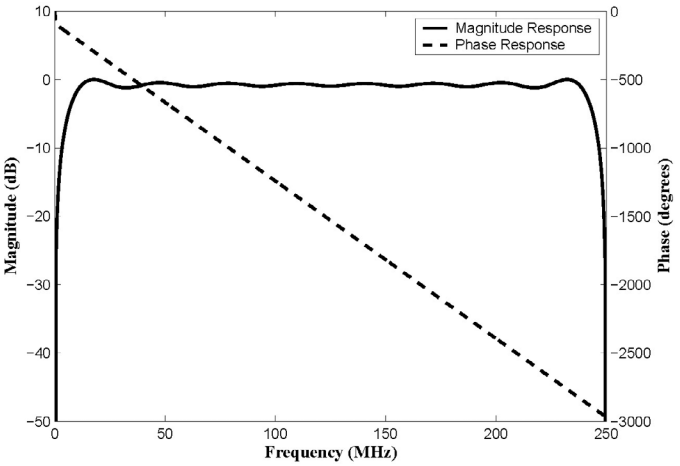

Fig. 3. Frequency responses of a 33-tap FIR Hilbert filter. Magnitude response (solid line) and phase response (dashed line).

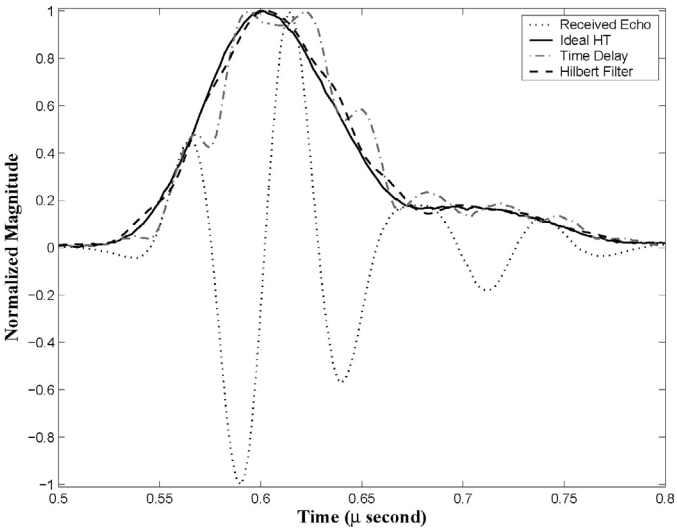

Fig. 4. Resultant the envelope information extracted by the time-delay method (gray dashed-dot line) and the Hilbert filter method (dashed line) compared with the outcome from the ideal Hilbert transformer (solid line).

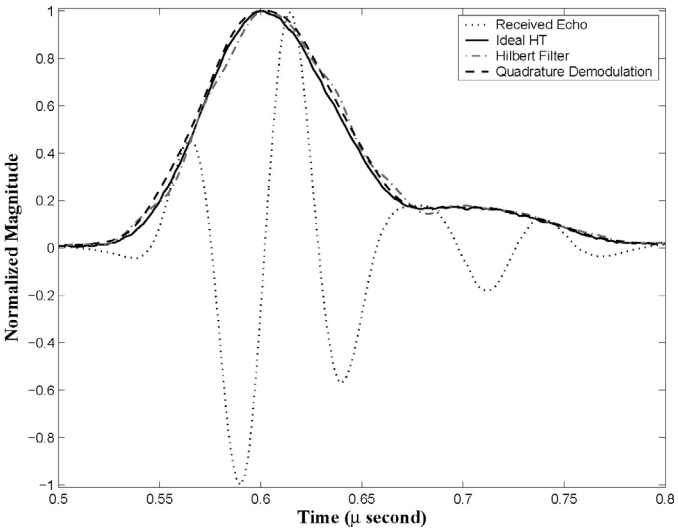

Fig. 5. Resultant the envelope information extracted by quadrature demodulation (dashed line) compared with the outcome from the Hilbert filter (gray dashed-dot line), and the ideal Hilbert transforming (solid line).

creased by using a large number of filter taps (more than a hundred). A drawback of this method is that it is difficult to remove the imbalance of two different signal paths, i.e., different frequency responses of a band pass filter (or all pass filter) and a Hilbert filter. This imbalance can be a more crucial problem in Doppler and color flow imaging rather than B-mode imaging.

Another approximate Hilbert transformer is obtained by delaying the original echo data by α samples corresponding to shifting a 90 degree phase from the center frequency of the received echo data as shown in Fig. 2(b) [3]. This method can provide acceptable accuracy when the received signal has a high quality factor Q, otherwise causing a serious error in the detected envelope [4]. Because the ultrasound pulse usually has a relatively low Q, a very fast sampling clock is required to use the time-delay method. This requirement is not easy to satisfy in high-frequency ultrasound imaging systems. In Fig. 4, it is plainly seen that the Hilbert filter method (dashed line) has a superior accuracy to the time-delay method (gray dashed-dot line) under the condition in which those envelope shapes fluctuate in the vicinity of the ideal envelope information (solid line). The normalized RMSE of the time-delay method was 17.60%, which is about three times higher than that of the Hilbert filter method, i.e., 6.21%. In addition to poor accuracy, the time-delay method cannot be used for Doppler and color flow imaging due to severe phase distortion. In this method, in fact, it is assumed that $A_I(nT_s) \approx A_I(nT_s - \alpha)$ and $A_Q(nT_s) \approx A_Q(nT_s - \alpha)$. Although the assumption is completely satisfied, time delay of α is the key factor resulting in the phase distortion of the Hilbert transformed signal.

D. Quadrature Demodulation

Quadrature demodulation is commonly used in Doppler and color flow imaging system [22], [23]. This method generates the baseband in-phase and quadrature component by mixing with sine and cosine waveforms and carrying out low pass filtering as shown in Fig. 2(c). The generated complex baseband components can be expressed as follows:

$$\begin{aligned} I(n) &= [r(n) \cdot \cos(n\omega_0 T_s)]_{\mathrm{LPF}} \\ &= \frac{K}{2} \cdot A(nT_s) \cdot \cos(\phi_n), \end{aligned} \tag{7}$$

$$\begin{aligned} Q(n) &= [r(n) \cdot \sin(n\omega_0 T_s)]_{\mathrm{LPF}} \\ &= -\frac{K}{2} \cdot A(nT_s) \cdot \sin(\phi_n), \end{aligned} \tag{8}$$

where K is the gain of LPF. With the complex baseband signals, finally, the envelope information is obtained by the following calculation:

$$E(n) = \sqrt{I(n)^2 + Q(n)^2} = \frac{K}{2} \cdot A(nT_s). \tag{9}$$

In Fig. 5, the results from the quadrature demodulation method (dashed line) and the Hilbert filter method (gray dashed-dot line) are presented to illustrate the accuracy of the two methods. The normalized RMSE of the quadrature demodulation method was 5.18%, which was the smallest value in the simulation. As a result, the Hilbert filter and the quadrature demodulation methods can be a candidate for the envelope detection algorithm in a high-frame rate, high-frequency ultrasound imaging system.

III. Description of Proposed Design

An envelope detector for the small animal cardiac imaging should satisfy the following requirements:

- The entire processing should be completed within at least 6.7 ms for a frame in order to support more than 150 frames per second.

- An implemented system based on an envelope detection algorithm should provide an accuracy within acceptable rounding error (i.e., less than 0.5) compared with these from the arithmetic computation of the algorithm.
- Phase information should be provided to a Doppler and color flow imaging block.

In order to satisfy these requirements, the proposed design adopts the quadrature demodulation method to extract the complex baseband signals, including the phase information, which is commonly used in Doppler and color flow imaging systems. The magnitude of the extracted complex baseband signals is computed by the square root function based on a new LUT strategy that can dramatically reduce the size of LUT through the manipulation of square rooting equation by using BLNS.

The LUT method for the implementation of (9) is capable of providing not only accuracy but also fast processing speed. However, the direct use of this method requires a tremendous amount of memory, thus manipulating (9) to reduce memory size is desirable. For this, the envelope signal can be rewritten by:

$$\begin{aligned} E(n) &= |Q(n)| \cdot \sqrt{1 + \left(\frac{I(n)}{Q(n)}\right)^2} \\ &= |Q(n)| \cdot \left(\sqrt{1 + \left(2^{\log_2(I(n)) - \log_2(Q(n))}\right)^2}\right). \end{aligned} \quad (10)$$

By applying the base 2 logarithm to (10), the logarithmic envelope signal then is obtained as follows:

$$\begin{aligned} \log_2[E(n)] &= \log_2(|Q(n)|) \\ &\quad + \log_2\left(\sqrt{1 + \left(2^{\log_2(I(n)) - \log_2(Q(n))}\right)^2}\right), \end{aligned} \quad (11)$$

where $\log_2(\bullet)$ represents BLNS, which is an alternative way to represent binary numbers capable of simplifying the computation of multiplication and division to addition and subtraction, respectively [13], [14]. A number of studies have shown the efficiency of BLNS in real-time digital signal processing applications in terms of processing time as well as accuracy [15]–[17]. In (11), therefore, the result from a subtraction operation between $\log_2(I(n))$ and $\log_2(Q(n))$ instead of a division operation is used as an input to a LUT containing the square rooting values and generating its outcomes in BLNS.

In a digital circuit, any positive decimal integer number N can be represented by an m-bit fixed-point number as follows:

$$\begin{aligned} N &= \sum_{i=0}^{m-1} b_i \cdot 2^i = b_l \cdot 2^l + \sum_{i=0}^{l-1} b_i \cdot 2^i \\ &= 2^l \left(1 + \sum_{i=0}^{l-1} b_i \cdot 2^{i-l}\right), \end{aligned} \quad (12)$$

where $b_i \in \{1, 0\}$ and l is the most significant bit position at which $b_l = 1$. Once the base 2 logarithm is applied to number N in order to convert it to a binary logarithmic number, (12) can be rewritten as:

$$\log_2(N) = l + \log_2\left(1 + \sum_{i=0}^{l-1} b_i \cdot 2^{i-1}\right). \quad (13)$$

Therefore, the integer and fractional values of $\log_2(N)$ are l and the second term of (13), respectively. For example, $\log_2(14_{10}) = \log_2(00001110_2) = 11.110100_2 = 3.8125_{10}$ with rounding. The real value of $\log_2(14)$ is 3.8074, so that error between the true and the 8-bit binary logarithmic values of the number 14 is less than 2^{-6}, which is a 0.13% difference.

Because the proposed design uses both the fixed-point number system and BLNS, the conversion between two different number systems as illustrated by (13) is required. It can be performed by means of either a LUT method [14], [18] or a computational method [19]. In the digital system requiring very fast processing time, the LUT method for both logarithmic and antilogarithmic conversion is used. Because the accuracy of antilogarithmic numbers is determined by the number of bits representing a binary logarithmic number, the conversion method based on LUT needs a large size memory to obtain precise antilogarithmic numbers. However, the proposed design does not involve the antilogarithmic conversion because the outcome of (11) represented by BLNS is directly used for logarithmic compression. For the reason, a logarithmic number can be also represented by the relatively small number of bits so that LUT can be served as the conversion method with a feasible memory size.

LOG-compressor plays the role in reducing the large dynamic range of received echo signals for efficient visualization. If an 8-bit gray scale LOG-compressor is applied to the envelope information $E(n)$, the compressed envelope data $r_{\text{env}}(n)$ in Fig. 2 can be written as [24]:

$$r_{\text{env}}(n) = \frac{20 \times 255}{\text{DR}} \cdot \left[\log_{10}\left(\frac{E(n)}{E_{\min}}\right)\right] + B, \quad (14)$$

where B is a gain factor and DR stands for dynamic range defined as the difference between the strongest and the weakest envelope data ($E_{\max}$ and $E_{\min}$) in logarithmic scale and can be expressed as $20 \cdot \log_{10}(E_{\max}) - 20 \cdot \log_{10}(E_{\min})$. By substituting (11) into (14), the LOG-compressed envelope data is given by:

$$\begin{aligned} r_{\text{env}}(n) = A \cdot \Bigg[&\log_2(Q(n)) \\ &+ \log_2\left(\sqrt{1 + \left(2^{\log_2(I(n)) - \log_2(Q(n))}\right)^2}\right) \\ &- \log_2(E_{\min})\Bigg] + B, \end{aligned} \quad (15)$$

where A is a LOG-compression constant and can be expressed as:

$$A = \frac{20 \times 255}{\text{DR} \cdot \log_2(10)}. \quad (16)$$

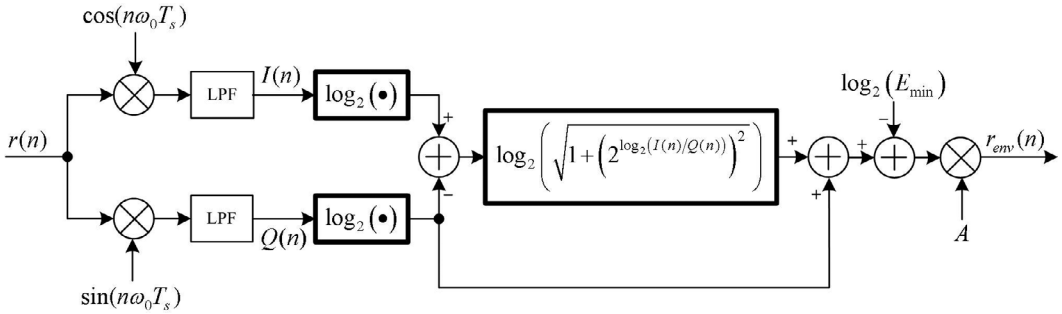

Fig. 6. Conceptual block diagram of the proposed design. A is a LOG-compression constant and $\log_2(E_{\min})$ is the weakest envelope value in logarithmic scale. Three bold boxes represent the look-up tables: two for the conversion from fixed-point numbers to binary logarithmic numbers and one for square root function.

Fig. 6 shows the conceptual block diagram of the proposed design expressed by (15), except the gain factor B for the sake of simplicity. The fixed-point numbers of both $I(n)$ and $Q(n)$ are converted to the binary logarithmic numbers through LUT depicted by two bold boxes containing base 2 logarithmic values represented by BLNS in Fig. 6. The result of a simple subtraction of $I(n)_{\mathrm{BLNS}}$ and $Q(n)_{\mathrm{BLNS}}$ is used as an input address to determine the output of LUT, which is a square root value expressed in the second term of (11). Once the dynamic range of enveloped echo signals is determined, the minimum envelope value in logarithmic scale is subtracted from the result of a simple addition between the outputs of LUT for the square root function and the quadrature component $Q(n)_{\mathrm{BLNS}}$. The LOG-compressed envelope information is obtained by multiplying the subtraction results by the LOG-compression constant. Although the gain factor B is not shown in Fig. 6, in addition, the system gain including one of LPF can be compensated by adding B to the LOG-compressed envelope information obtained. The conceptual block diagram can be implemented with hardware logic components as shown in Fig. 7, including remedies for the logarithmic representation of zero number and boundary detection.

If in-phase and quadrature components are represented by m-bit fixed-point numbers and converted to k-bit binary logarithmic numbers, two $2^m \times k$-bits memory for converting fixed-point numbers to binary logarithmic numbers ($\mathrm{LUT_A}$) and one $2^{k+1} \times k$-bit memory for the square root value ($\mathrm{LUT_B}$) are used in Fig. 7. Each hardware logic component has latency of one clock cycle except LUTs and boundary detectors of which latency is two clock cycles. Therefore, the latency for the square root function and the logarithmic compression becomes 15 clock cycles. The latency for the quadrature demodulation depends on the number of taps required for a LPF. If a 33-tap LPF is used to obtain a complex baseband component, outcomes from the LPF after 16 clock cycles $[(33-1) \div 2]$ can be regarded as a valid output set to maintain the same number of input and output samples, although it still contains transient output data. In this case, the latency for the quadrature demodulation is 17 clock cycles, including latency of one clock cycle for mixing echo signals with sine and cosine waveforms. As a result, the total latency of the proposed design is 32 clock cycles, so that a LOG-compressed envelope samples can be obtained at every clock cycle after 32 clock cycles.

By a maximum error analysis, the minimum number of bits representing binary logarithmic numbers can be determined so as to avoid the rounding error. The error of the proposed design arises from the conversion of baseband echo signals into binary logarithmic numbers to carry out the fast square root computation and logarithmic compression. If a logarithmic number is represented by I-bit integer and F-bit fractional parts, the maximum conversion error is $2^{-(F+1)}$ and thus both a subtraction and an addition of two binary logarithmic numbers generate the maximum error of 2^{-F}.

Because the outcome from the second term of (11) can be exactly calculated by a computer and stored in $\mathrm{LUT_B}$ with $2^{-(F+1)}$ error, its maximum error is still equal to 2^{-F} arising from the subtraction of $\log_2(I(n))$ and $\log_2(Q(n))$. As a result, the maximum error of the proposed design can be expressed as:

$$\begin{aligned} \mathrm{err}_{\max} &= A_{\max} \cdot \Big\{ \mathrm{err}\left[\log_2(Q(n))\right] + \mathrm{err}[\mathrm{LUT}_B] \\ &\qquad + \mathrm{err}\left[\log_2(E_{\min})\right] \Big\} \\ &= A_{\max} \cdot 2^{-(F+1)} + A_{\max} \cdot 2^{-F} + A_{\max} \cdot 2^{-(F+\beta)} \\ &= A_{\max} \cdot 2^{-F} + A_{\max} \cdot 2^{-F} \cdot \left[2^{-1} + 2^{-\beta}\right], \end{aligned} \tag{17}$$

where $\mathrm{err}[\bullet]$ is a function for computing the maximum error, β is the number of extra fractional bits assigned to $E_{\min}$ in BLNS, and $A_{\max}$ is a possible maximum integer value of the LOG-compression constant. If DR is greater than or equal to 48 dB, $A_{\max}$ becomes 32 (2^5) and thus (17) can be rewritten by:

$$\mathrm{err}_{\max} = 2^{-F+5} + 2^{-F+5} \cdot \left[2^{-1} + 2^{-\beta}\right]. \tag{18}$$

If β is greater than 1 and F is greater than 7, the maximum error is always less than 0.5, i.e., within the rounding error. Because the maximum error analysis tends to overestimate the error of a system, the number of bits of the fractional part in BLNS can be assigned to 6 instead of 7 in spite of the maximum error of 0.875, which rarely occurs.

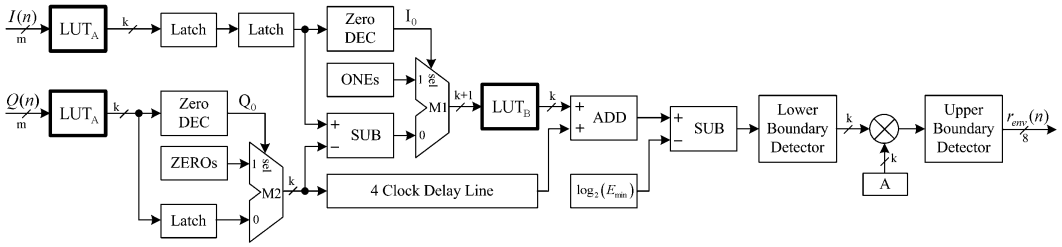

Fig. 7. Hardware logic description to extract the LOG-compressed envelope information from the complex baseband components represented by an m-bit fixed-point number, which is converted to a k-bit binary logarithmic number through $\mathrm{LUT_A}$. The square root values are generated through $\mathrm{LUT_B}$. The proposed envelope detector generates 8-bit resultant data going to a digital scan converter in which gray-level images are displayed on a monitor.

The number of bits of the integer part in BLNS, I, is determined by the number of bits used to represent fixed-point numbers, i.e., ceil[$\log_2$ (number of bits)] where a function of ceil[•] returns the smallest integer value no less than its input value. If $I(n)$ and $Q(n)$ in (9) are represented by the 16-bit fixed-point number system, therefore, the number of bits of integer and fractional parts in BLNS is 4 bits and 6 bits, respectively. The total number of bits for BLNS is therefore 10 bits. From this result, the memory size for the conversion is 164 Kbytes ($2 \times 2^{16} \times 10 \div 8$) and it for square root function generating 10-bit outcomes is 2.56 Kbytes ($2^{11} \times 10 \div 8$) considering a sign bit resulting from the subtraction. Therefore, a total of 166.56 Kbytes memories are used for the proposed design. This is a noticeably reduced size of memory, compared with a 4 Gbytes ($2^{32} \times 8 \div 8$) size of memory in the fixed-point number system. Through the change of the number system, furthermore, the LOG-compression functional block can be removed and merged with the proposed envelope detector.

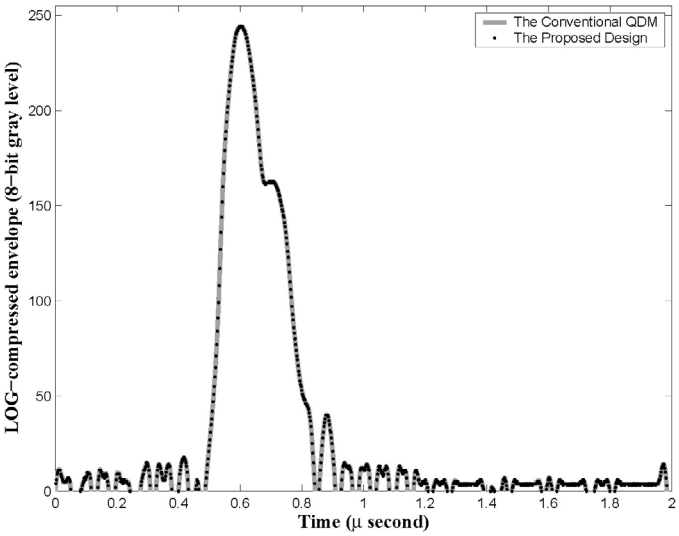

Fig. 8. Comparison of the accuracy of the proposed design (dots) adopting 10-bit BLNS with that of the conventional quadrature demodulation method (gray solid line).

IV. Results

The validation of the proposed design was achieved by comparing its outcome with that of the conventional quadrature demodulation method using MATLAB (MathWorks Inc., Natick, MA). For the sake of comparison, the envelope information of the conventional quadrature demodulation shown in Fig. 5 was logarithmically compressed to a 48 dB dynamic range. The proposed design used the same LPFs and sine/cosine data as those used for the conventional quadrature demodulation in Section II. The total number of bits for BLNS was 10 consisting of a 4-bit integer part and a 6-bit fractional part in which the word sign bit was removed because only the magnitude of each of the complex baseband component contributes to obtaining the envelope information. Fig. 8 shows the LOG-compressed envelope data represented by 8-bit gray level obtained by the conventional quadrature demodulation (gray solid line) and the proposed method (dotted line) adopting 10-bit BLNS. The maximum difference between the two methods was 0.476, which was within the rounding error. Once the fractional part of BLNS was assigned to 7 bits so as to make 11-bit BLNS, the maximum difference was reduced to 0.237. In addition, the normalized RMSE of the proposed design with 10-bit BLNS and LOG-compressed version of the ideal Hilbert transformer shown in Section II was 7.472%, which was less than that of the conventional quadrature demodulation with ideal LOG compression, i.e., 7.473%. In fact, LOG compression may increase the normalized RMSE value of a certain system. From the results, it is seen that the proposed envelope detector is capable of providing the same functionality as the conventional quadrature demodulation with negligible quantization error, i.e., within rounding error.

The hardware implementation of the proposed design shown in Fig. 7 was carried out in a FPGA (Stratix EP1S60F1020C6, Altera Corporation, San Jose, CA) on a test board operating at 100 MHz. The specifications in the hardware implementation were the same as those for MATLAB simulation, except for the echo signal. A single scan vector consisting of 8-bit 2048 samples was obtained from a rabbit eyeball with a 20-MHz single element transducer as shown in the top panel of Fig. 9, and it contained a fundamental component of about 20 MHz bandwidth and a second harmonic component at −35 dB level. The single scan vector was stored in the FPGA internal memory to calculate the operating time of the proposed de-

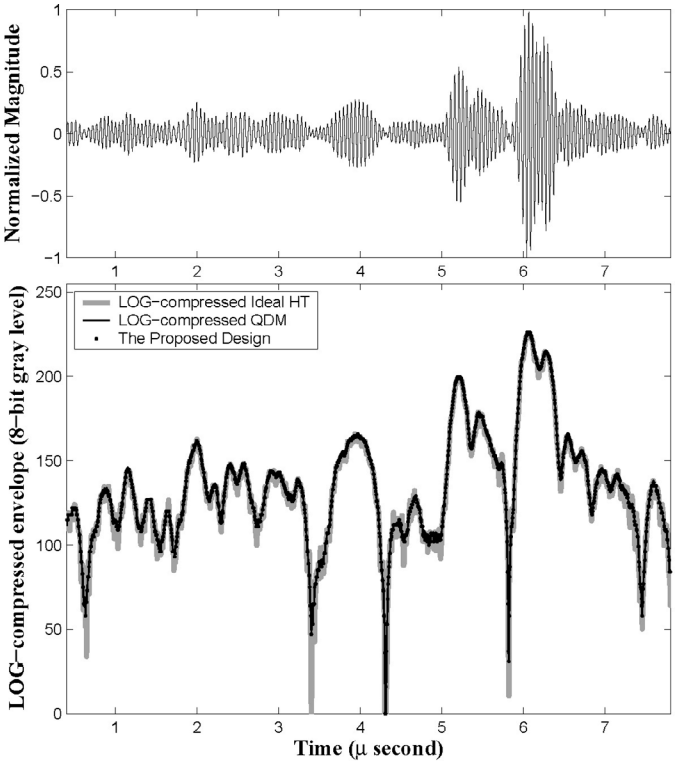

Fig. 9. LOG-compressed envelope information extracted by the proposed design implemented in FPGA (dots in the bottom panel). The resultant envelope shape from the proposed design is compared with those of the ideal Hilbert transformer (gray solid line in the bottom panel) and of the conventional quadrature demodulation (dashed line) obtained on MATLAB. The top panel shows a single scan vector acquired from a rabbit eyeball obtained by a 20-MHz, single-element transducer.

sign. Whenever an external trigger signal comes into the test board, the memory containing the single scan vector starts to send the stored data to the envelope detector module, which starts its task by the external trigger signal as well. Theoretically, a total of 2080 clock cycles, including 32 clock cycle latency, are needed to perform the envelope detection for the single scan vector, so that the fastest triggering frequency should be about 48.1 KHz at the operating clock of 100 MHz. In the experiment, as expected, the highest triggering frequency was 48 KHz, corresponding to a 20.8 μs operating time needed to extract the envelope information from the echo signal comprised of 2048 samples. If a frame consists of 256 scanlines, the total time to obtain the LOG-compressed envelope samples of the frame is 5.3 ms in the proposed design, thus satisfying the requirement for the processing time. As a result, it is obviously seen that the proposed design can be used for very high-frame rate, high-frequency ultrasound system generating more than 150 frames per second.

In the bottom panel of Fig. 9, it is shown that the LOG-compressed envelope extracted by the proposed design implemented in hardware (dots) is the same as that by the conventional quadrature demodulation (dashed line) obtained from MATLAB simulation. The maximum error of the proposed design compared with the conventional quadrature demodulation with ideal logarithmic compression was 0.465, which should be negligible in practice. In addition, the normalized RMSE between the envelope data of the proposed design and the ideal Hilbert transformer obtained from MATLAB simulation (gray solid line in the bottom panel of Fig. 9) was 5.177%, which was similar to that of the conventional quadrature demodulation. Because the low pass filtering in the quadrature demodulation discards high-frequency components of the original echo signal, the fluctuated portion on the LOG-compressed envelope signal from the ideal Hilbert transformer becomes smoother. In B-mode image, however, this phenomenon should not affect the image quality much because meaningful information such as tissue structures still can be obtained from the overall shape of the envelope signal. This can be confirmed by the B-mode images of a formalinized pig eyeball shown in Fig. 10.

The formalinized pig eyeball was linearly scanned by using an ultrasound biomicroscope (UBM) system with a 50-MHz signal element transducer that has a −6 dB bandwidth of 55% and a focal distance of 6 mm (1.4 f-number). Echo signals were sampled by using 14-bit ADC (CS14200, Gage Applied Technologies, Montreal, Quebec, Canada) at 200 MHz. A frame was composed of 400 scanlines and 2048 samples per scanline. Envelope information was logarithmically compressed to a 60 dB dynamic range. The image produced by the proposed design shown in Fig. 10(b) provides information about the anterior segment of the eye such as the cornea, the iris, and the lens as clearly as that by the ideal Hilbert transformer shown in Fig. 10(a).

V. Conclusions

A high-frame rate, high-frequency ultrasound imaging system requires not only very fast data acquisition but also fast signal processing to generate images in real time. This paper has proposed a novel design of envelope detectors capable of supporting the small animal cardiac imaging system requiring very high-frame rate (more than 150 frames per second). To achieve very fast operating speed as well as good accuracy, a new way that uses LUT for obtaining the square root function by computing the magnitude of the complex baseband components extracted from the quadrature demodulation has been proposed. The new LUT strategy with BLNS has the advantage of reducing the size of LUT, thus enabling us to take advantage of the attractive properties of the LUT method that allows a fast operating speed, high accuracy, and simple implementation. The performance of the proposed design was examined, and the results have shown that the proposed design is suitable for envelope detection in a high-frame rate, high-frequency ultrasound imaging system in terms of operating speed and accuracy. In fact, the new LUT strategy with BLNS described in this paper is a versatile method for the system requiring very fast operation speed. For example, this method can be used for a very fast dig-

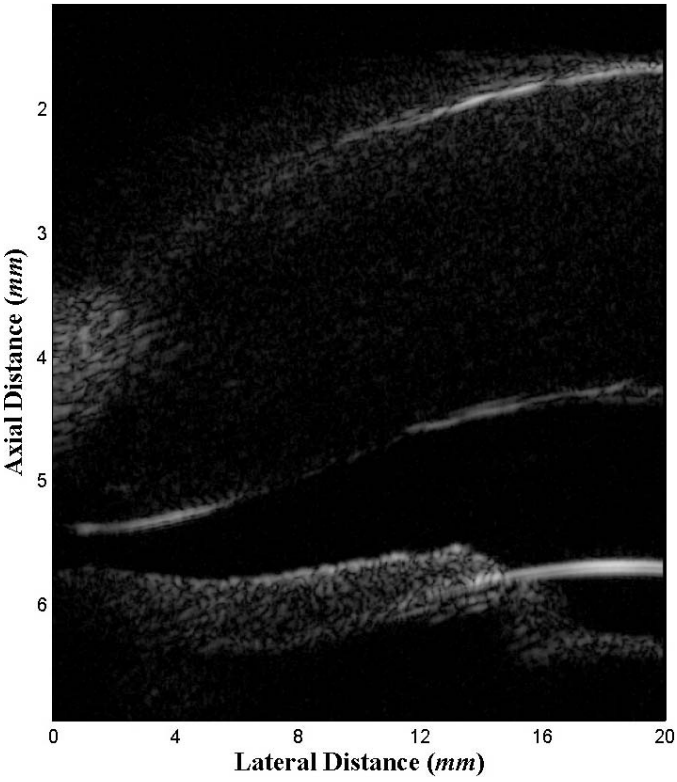

(a)

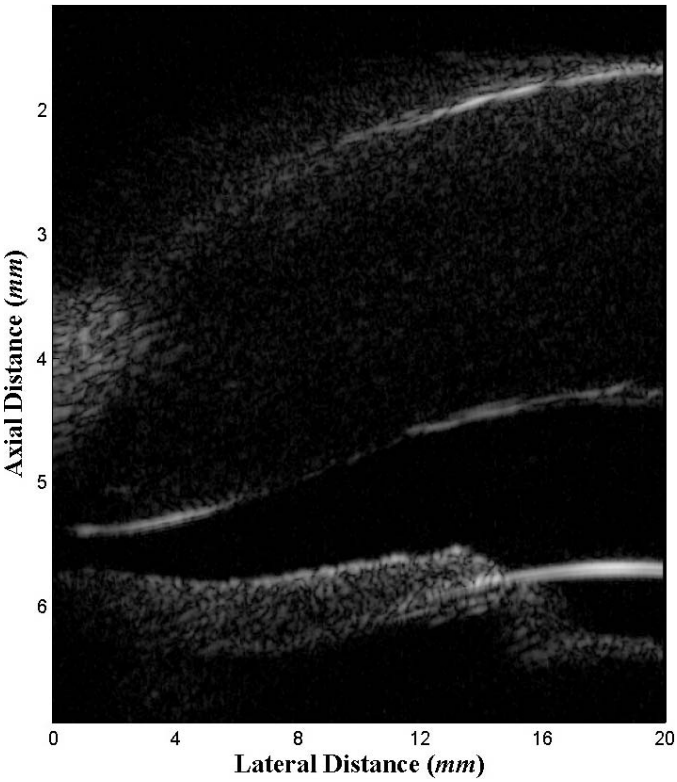

(b)

Fig. 10. B-mode images of the excised pig eyeball involving the ideal Hilbert transformer (a) and the proposed design (b). The images have a 60-dB dynamic range and its focal depth is 6 mm.

ital scan converter performing coordinate conversion from Cartesian coordinate to polar coordinate.

References

[1] B. G. Tomov and J. A. Jensen, "Compact FPGA-based beamformer using oversampled 1-bit A/D converters," *IEEE Trans. Ultrason., Ferroelect., Freq. Contr.*, vol. 52, no. 5, pp. 870–880, 2005.

[2] I. Kollár, R. Pintelon, and J. Schoukens, "Optimal FIR and IIR Hilbert transformer design via LS and minimax fitting," *IEEE Trans. Instrum. Meas.*, vol. 39, no. 6, pp. 847–852, 1990.

[3] M. Schlaikjer, J. P. Bagge, O. M. Sorensen, and J. A. Jensen, "Trade off study on different envelope detectors for B-mode imaging," in *Proc. IEEE Ultrason. Symp.*, 2003, pp. 1938–1941.

[4] T. K. Song and S. B. Park, "A new digital phased array system for dynamic focusing and steering with reduced sampling rate," *Ultrason. Imag.*, vol. 12, pp. 1–16, 1990.

[5] S. Sikdar, R. Managuli, L. Gong, V. Shamdasani, T. Mitake, T. Hayashi, and Y. Kim, "A single media processor-based programmable ultrasound system," *IEEE Trans. Inform. Technol. Biomed.*, vol. 7, no. 1, pp. 64–70, 2003.

[6] H.-C. Kim, H.-Y. Sohn, J.-H. Sim, and T.-K. Song, "An optimized software-based echo-processing algorithm for small scale ultrasound systems," in *Proc. IEEE Ultrason. Symp.*, 2004, pp. 2053–2056.

[7] P. Montuschi and M. Mezzalama, "Survey of square rooting algorithms," *Proc. IEEE*, vol. 137, no. 1, pp. 31–40, 1990.

[8] J. E. Volder, "The CORDIC trigonometric computing technique," *IRE Trans. Electron. Comput.*, vol. 8, pp. 330–334, 1959.

[9] J. Prado and R. Alcantara, "A fast square-rooting algorithm using a digital signal processor," *Proc. IEEE*, vol. 75, no. 2, pp. 262–264, 1987.

[10] X. C. Xu, C. H. Hu, L. Sun, J. Yen, and K. K. Shung, "High-frequency high frame rate ultrasound imaging system for small animal imaging with linear array," in *Proc. IEEE Ultrason. Symp.*, 2005, pp. 1431–1434.

[11] F. S. Foster, G. Liu, J. Mehi, B. S. Starkoski, L. Adamson, Y. Zhow, K. A. Harasiecwicz, and L. Zan, "High frequency ultrasound imaging: From man to mouse," in *Proc. IEEE Ultrason. Symp.*, 2000, pp. 1633–1638.

[12] C.-H. Hu, X.-C. Xu, J. M. Cannata, J. T. Yen, and K. K. Shung, "Development of a real-time, high-frequency ultrasound digital beamformer for high-frequency linear array transducers," *IEEE Trans. Ultrason., Ferroelect., Freq. Contr.*, vol. 53, no. 2, pp. 317–323, 2006.

[13] I. Koren, *Computer Arithmetic Algorithms*. 2nd ed. Natick, MA: A. K. Peters, 2002.

[14] H.-Y. Lo and Y. Aoki, "Generation of a precise binary logarithm with difference grouping programmable logic array," *IEEE Trans. Comput.*, vol. C-34, no. 8, pp. 681–691, 1985.

[15] T. Kurokawa, J. A. Payne, and S. C. Lee, "Error analysis of recursive digital filters implemented with logarithmic number system," *IEEE Trans. Acoust. Speech Signal Processing*, vol. ASSP-28, no. 6, pp. 706–715, 1980.

[16] O. Vainio and Y. Neuvo, "Logarithmic arithmetic in FIR filters," *IEEE Trans. Circuits Syst.*, vol. CAS-33, no. 8, pp. 826–828, 1986.

[17] F. J. Taylor, R. Gill, J. Joseph, and J. Radke, "A 20 bit logarithmic number system processor," *IEEE Trans. Comput.*, vol. 37, no. 2, pp. 190–200, 1988.

[18] Y. Wan and C. L. Wey, "Efficient algorithms for binary logarithmic conversion and addition," *IEE Proc. Comp. Digit. Tech.*, vol. 146, no. 3, pp. 168–172, 1999.

[19] K. H. Abed and R. E. Siferd, "CMOS VLSI implementation of a low-power logarithmic converter," *IEEE Trans. Comput.*, vol. 52, no. 11, pp. 1421–1433, 2003.

[20] A. D. Poularikas and S. Seely, *Signals and Systems*. 2nd ed. Melbourne, FL: Krieger, 1994.

[21] J. A. Brown and G. R. Lockwood, "A digital beamformer for high-frequency annular arrays," *IEEE Trans. Ultrason., Ferroelect., Freq. Contr.*, vol. 52, no. 8, pp. 1262–1269, 2005.

[22] T. L. Szabo, *Diagnostic Ultrasound Imaging: Inside Out*. San Diego, CA: Elsevier Academic, 2004, ch. 11.

[23] H. J. Nitzpon, J. C. Rajaonah, C. B. Burckhardt, B. Dousse, and J. J. Meister, "A new pulsed wave Doppler ultrasound system to measure blood velocities beyond the Nyquist limit," *IEEE Trans. Ultrason., Ferroelect., Freq. Contr.*, vol. 42, no. 2, pp. 265–279, 1995.

[24] D. Kaplan and Q. Ma, "On the statistical characteristics of log-compressed Rayleigh signals: Theoretical formulation and experimental results," *J. Acoust. Soc. Amer.*, vol. 95, no. 3, pp. 1369–1400, 1994.

Jin Ho Chang (S'00) was born in Seoul, South Korea, November 1973. He received his B.S. and M.S. degrees in electronic engineering from Sogang University, Seoul, South Korea, in 2000 and 2002, respectively. From 2002 through 2003, he worked at the Digital Media Research Lab., LG Electronics Inc., Seoul, South Korea, as a research engineer. He is currently a Ph.D. candidate at the Department of Biomedical Engineering, University of Southern California, Los Angeles, CA.

His research interests include the development of a high-frequency ultrasound imaging system, ultrasound signal processing, and ultrasound field analysis. He is a student member of the Institute of Electrical and Electronics Engineers (IEEE).

Jesse T. Yen (M'03) was born in Houston, TX, on September 23, 1975. He received B.S.E. and Ph.D. degrees in biomedical engineering from Duke University, Durham, NC, in 1997 and 2003, respectively. He is currently an assistant professor in the biomedical engineering department at the University of Southern California, Los Angeles, CA.

His research interests include two-dimensional array design and fabrication, three-dimensional ultrasound, three-dimensional elastography, and high frequency ultrasound systems.

K. Kirk Shung (S'73–M'75–SM'89–F'93) obtained a B.S. degree in electrical engineering from Cheng-Kung University in Taiwan in 1968, an M.S. degree in electrical engineering from the University of Missouri, Columbia, MO, in 1970 and a Ph.D. degree in electrical engineering from the University of Washington, Seattle, WA, in 1975. He did postdoctoral research at Providence Medical Center in Seattle, WA, for 1 year before being appointed a research bioengineer holding a joint appointment at the Institute of Applied Physiology and Medicine, Seattle, WA. He became an assistant professor at the Bioengineering Program, Pennsylvania State University, University Park, PA, in 1979 and was promoted to professor in 1989. He was a Distinguished Professor of Bioengineering at Penn State until September 1, 2002, when he joined the Department of Biomedical Engineering, University of Southern California, Los Angeles, CA, as a professor. He has been the director of NIH Resource on Medical Ultrasonic Transducer Technology since 1997.

Dr. Shung is a fellow of the IEEE, the Acoustical Society of America, and the American Institute of Ultrasound in Medicine. He is a founding Fellow of the American Institute of Medical and Biological Engineering. He has served for two terms as a member of the NIH Diagnostic Radiology Study Section. He received the IEEE Engineering in Medicine and Biology Society early career award in 1985 and was the co-author of a paper that received the best paper award for *IEEE Transactions on Ultrasonics, Ferroelectrics, and Frequency Control* (UFFC) in 2000. He was the distinguished lecturer for the IEEE UFFC society for 2002–2003. He was elected an outstanding alumnus of Cheng-Kung University in Taiwan in 2001.

Dr. Shung has published more than 200 papers and book chapters. He is the author of a textbook, *Principles of Medical Imaging,* published by Academic Press in 1992 and a text book, *Diagnostic Ultrasound: Imaging and Blood Flow Measurements,* published by CRC Press in 2005. He co-edited a book, *Ultrasonic Scattering by Biological Tissues,* published by CRC Press in 1993. Dr. Shung's research interest is in ultrasonic transducers, high-frequency ultrasonic imaging, and ultrasonic scattering in tissues.